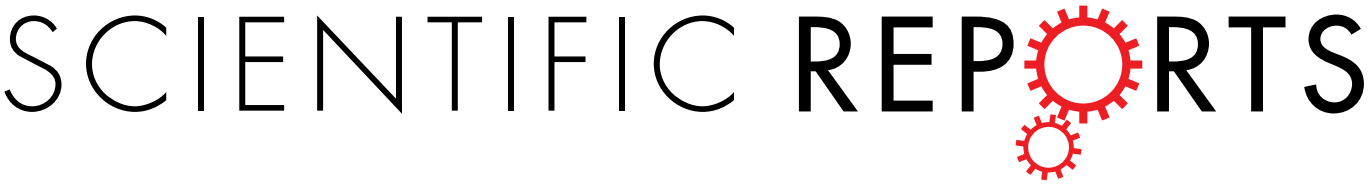

OPEN

A New Generation of Arachidonic Acid Analogues as Potential Neurological Agent Targeting Cytosolic Phospholipase A_2

Received: 30 June 2017
Accepted: 4 October 2017
Published online: 20 October 2017

Cheng Yang Ng[1], Srinivasaraghavan Kannan[2], Yong Jun Chen[3], Francis Chee Kuan Tan[4], Wee Yong Ong[1], Mei Lin Go[3], Chandra S. Verma[2], Chian-Ming Low[4,5] & Yulin Lam[1]

Cytosolic phospholipase A_2 ($cPLA_2$) is an enzyme that releases arachidonic acid (AA) for the synthesis of eicosanoids and lysophospholipids which play critical roles in the initiation and modulation of oxidative stress and neuroinflammation. In the central nervous system, $cPLA_2$ activation is implicated in the pathogenesis of various neurodegenerative diseases that involves neuroinflammation, thus making it an important pharmacological target. In this paper, a new class of arachidonic acid (AA) analogues was synthesized and evaluated for their ability to inhibit $cPLA_2$. Several compounds were found to inhibit $cPLA_2$ more strongly than arachidonyl trifluoromethyl ketone ($AACOCF_3$), an inhibitor that is commonly used in the study of $cPLA_2$-related neurodegenerative diseases. Subsequent experiments concluded that one of the inhibitors was found to be $cPLA_2$-selective, non-cytotoxic, cell and brain penetrant and capable of reducing reactive oxygen species (ROS) and nitric oxide (NO) production in stimulated microglial cells. Computational studies were employed to understand how the compound interacts with $cPLA_2$.

Phospholipases A_2 (PLA_2s) are a superfamily of enzymes characterized by their ability to hydrolyze the ester bond at the *sn*-2 position of glycerophospholipids to yield polyunsaturated fatty acids (PUFAs) and a lysophospholipid[1]. The mammalian PLA_2 family comprises six main types of enzymes, namely the secreted small molecular weight $sPLA_2$, the larger cytosolic Ca^{2+}-dependent $cPLA_2$, the Ca^{2+}-independent $iPLA_2$, the platelet-activating factor acetylhydrolases PAF-AH and the lysosomal PLA_2. Of these PLA_2 enzymes, the ubiquitous $cPLA_2$ is found to be responsible for the release of arachidonic acid (AA), an important PUFA which serves as the precursor for the synthesis of eicosanoids and prostanoids that mediate a wide variety of inflammatory responses[2]. In the central nervous system, $cPLA_2$ activation has been implicated in the pathogenesis of a number of neurodegenerative (Alzheimer's disease, Parkinson's disease and prion diseases) and neuropsychiatric (schizophrenia and depressive disorder) diseases[3–7]. Effects of neuroinflammation and its involvement in nitrosative/oxidative signaling pathways for example have been frequently cited as a pathogenetic link to Aβ-amyloid production due to the actions of $cPLA_2$[8]. A direct effect of sustained and aberrant $cPLA_2$ activation could result in enhanced neural membrane destruction eventually compromising functions on membrane ion receptors, leading to cell death[3–7]. Thus $cPLA_2$ is an important target for drug discovery, and for the development of new therapeutics to treat neurodegenerative and neuropsychiatric disorders. An ideal $cPLA_2$ inhibitor should not only reach the site where inflammatory processes are taking place (this may be achieved through improved drug delivery systems), they should also inhibit inflammation, block oxidative stress and cross the blood-brain barrier (BBB). To-date, various compounds have been shown to inhibit $cPLA_2$ selectively[9–16]. However many of these compounds have not yet been shown

[1]Department of Chemistry, National University of Singapore, 3 Science Drive 3, Singapore, 117543, Singapore. [2]Bioinformatics Institute, Agency for Science, Technology and Research (A*STAR), Matrix, Singapore, 138671, Singapore. [3]Department of Pharmacy, National University of Singapore, 21 Lower Kent Ridge Road, Singapore, 119077, Singapore. [4]Department of Anaesthesia, Yong Loo Lin School of Medicine, National University of Singapore, 5 Lower Kent Ridge Road, Singapore, 119074, Singapore. [5]Department of Pharmacology, Yong Loo Lin School of Medicine, National University of Singapore, 16 Medical Drive, Singapore, 117600, Singapore. Correspondence and requests for materials should be addressed to C.S.V. (email: chandra@bii.a-star.edu.sg) or C.-M.L. (email: phclowcm@nus.edu.sg) or Y.L. (email: chmlamyl@nus.edu.sg)

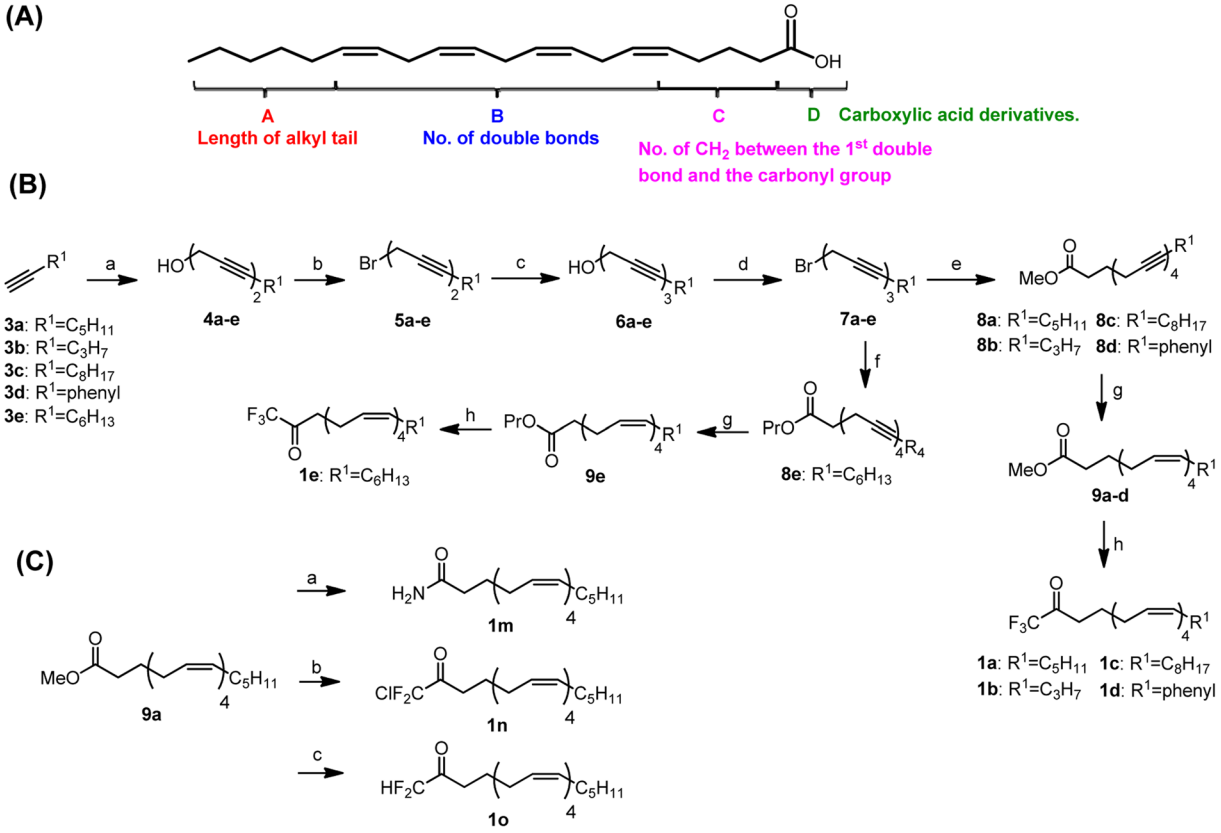

Figure 1. (**A**) Functionalities on AA that could be varied. (**B**) Reagent and conditions: (a) 4-Chloro-2-butyn-1-ol, CuI, NaI, K_2CO_3, DMF, rt, overnight (b) CBr_4, PPh_3, CH_2Cl_2, −40 °C to −20 °C, 1 h (c) Propargyl alcohol, CuI, NaI, K_2CO_3, DMF, rt, overnight (d) CBr_4, PPh_3, CH_2Cl_2, −40 °C to −20 °C, 1 h (e) Methyl 6-hexynoate, CuI, NaI, K_2CO_3, DMF, rt, overnight (f) Propyl 5-pentynoate, CuI, NaI, K_2CO_3, DMF, rt, overnight (g) H_2, $Ni(OAc)_2.4H_2O$, $NaBH_4$, en, 95% EtOH, rt, 2 h (h) i) NaOH, MW 120 °C, 1 h ii) Trifluoroacetic anhydride, Pyridine, CH_2Cl_2, rt, 2 h (**C**) (a) NH_3, $Mg(OMe)_2$, MeOH, 80 °C, overnight (b) i) NaOH, MW 120 °C, 1 h ii) Chlorodifluoroacetic anhydride, Pyridine, CH_2Cl_2, rt, overnight (c) i) NaOH, MW 120 °C, 1 h ii) Difluoroacetic anhydride, Pyridine, CH_2Cl_2, rt, overnight.

to possess brain penetrability[17,18]. Thus as part of our efforts to develop $cPLA_2$ inhibitors as potential drug candidates for the treatment of neurological disorders, we have synthesized a new series of AA analogues **1**–**2** and evaluated them for their PLA_2 inhibitory activities and ability to cross the BBB. In our inhibitor design, we have focused on the arachidonyl scaffold as earlier studies have shown that this pharmacophore is strongly recognized by $cPLA_2$[19–23]. We herein present the synthesis of AA analogues **1**–**2** and the investigation of these compounds for their (i) inhibition of $cPLA_2$, (ii) cytotoxicity, (iii) selectivity and anti-neuroinflammatory properties and (iv) ability to cross the blood-brain barrier; finally computational studies were performed to understand how the compounds bind to $cPLA_2$.

Results and Discussion

Chemistry. Using AA as a scaffold, our inhibitor design involved modification at different selected positions of the compound (Fig. 1A). In particular, the carboxylic acid functionality could be modified to a trifluoromethylketone group to form the well-known $cPLA_2$ inhibitor, $AACOCF_3$. Being cell penetrant, $AACOCF_3$ has been effective in reducing the undesirable effects of dysregulated $cPLA_2$ systems, including those found in neurological diseases[9,24–26]. A series of compound with the CF_3 moiety was synthesized and presented as compound **1**.

Compound **1** was prepared by assembling the alkynes together through a series of coupling and bromination reactions according to the synthetic strategy shown in Fig. 1B[27–30]. A total of 3 coupling and 2 bromination reactions were performed to reach the skipped diynes **8a**–**e** (4 alkynes) and **10a**–**c** (3 alkynes). Compound **8a** was initially hydrogenated with Brown's P2 nickel catalyst in ethanol according to a published procedure[27]. However this did not provide the desired compound **9a**. Optimization of the hydrogenation reaction by varying the equivalent of the catalyst and reaction conditions eventually provided **9a** in 68% yield (Supplementary Table S1). Initial attempts to trifluoromethylate **9a** by stirring $TMSCF_3$ and CsF as a TMS activator with the ester in $CHCl_3$ at room temperature did not yield **1a** ($AACOCF_3$)[31]. Replacing CsF with TBAF also failed to provide the desired compound[32]. We attempted to convert **9a** to the corresponding carboxylic acid and then treating it with LDA and EtO_2CCF_3[33]. However this too did not yield **1a**. Finally we trifluoromethylated the intermediate carboxylic

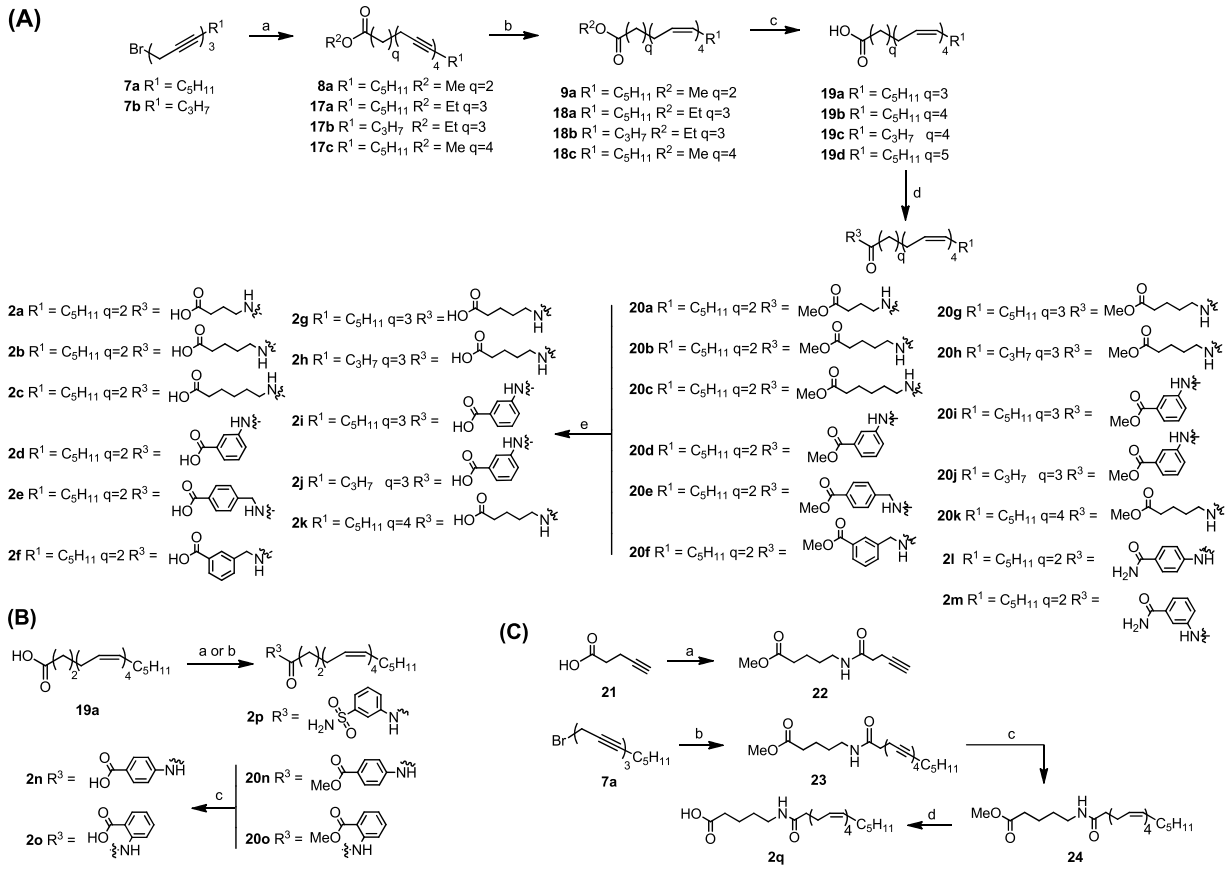

Figure 2. (**A**) Reagent and conditions: (a) $CH{\equiv}C\text{-}(CH_2)_qCO_2R^2$, CuI, NaI, K_2CO_3, DMF, rt, overnight (b) H_2, $Ni(OAc)_2.4H_2O$, $NaBH_4$, en, 95% EtOH, rt, 2 h (c) MeOH/NaOH, rt, 3 h (d) NH_2-Alk-CO_2Me or NH_2-Ar-CO_2Me or NH_2-Ar-$CONH_2$, EDC.HCl, HOBt, TEA, DMF, rt, overnight e) MeOH/NaOH, rt, 3 h. (**B**) Reagent and conditions: (a) 3-aminobenzenesulfonamide, EDC.HCl, TEA, MeCN, 4 °C, overnight (b) i) ($COCl_2$), catalytic DMF, CH_2Cl_2, rt, 1 h ii) NH_2-Ar-CO_2Me, TEA, THF, rt, overnight (c) MeOH/NaOH, rt, 3 h. (**C**) Reagent and conditions: (a) Methyl 5-aminopentanoate hydrochloride, EDC.HCl, HOBt, TEA, DMF, rt, overnight (b) **22**, CuI, NaI, K_2CO_3, DMF, rt, overnight (c) H_2, $Ni(OAc)_2.4H_2O$, $NaBH_4$, en, 95% EtOH, rt, 2 h (d) MeOH/NaOH, rt, 3 h.

acid with pyridine and TFAA[34,35] and gratifyingly this gave **1a** in 48% yield (over 2 steps). Analogues **1b**–**1h** were synthesized in the same manner by varying alkyne **3** in the first step of the reaction (Supplementary Scheme S1).

In the synthesis of **1i**–**l**, the precursor intermediates **13a**–**d** are not commercially available and were synthesized by treating alkyl halides **12a**–**d** with propargyl alcohol in the presence of butyllithium and an additive as a solvating agent. Initially *N*,*N*'-dimethylpropyleneurea (DMPU) was used as the additive but it gave **13b** in only 20% yield. Hence we tried hexamethylphosphoramide (HMPA) which provided **13b** in 86% yield. This may be attributed to the increased polarity of the P=O bond in HMPA as compared to the C=O in DMPU which stabilizes the acetylide to a greater extent. HMPA was thus used as an additive for the synthesis of intermediates **13a**–**d**. To form the primary amide **1m**, tetraene **9a** was amidated by heating it overnight at 80 °C in a solution of ammonia dissolved in methanol and $Mg(OMe)_2$. The chlorodifluoroketo and difluoroketo functionalities in **1n** and **1o** were respectively synthesized by hydrolyzing the ester **9a** to the corresponding carboxylic acid followed by a reaction with the respective anhydrides in pyridine and dichloromethane at room temperature (Fig. 1C).

Compound **2** differs from **1** as it contains an extension from the carbonyl amide. **2** was synthesized by first coupling the skipped dyne **7a** and **7b** with the respective alkynes to form **8a** and **17a**–**c** (Fig. 2). Subsequent hydrogenation and ester hydrolysis gave the corresponding carboxylic acids **19a**–**d** which were then coupled to the appropriate amines using EDC.HCl, HOBt, and TEA to give **20a**–**20k**, **2l**–**2m**. Coupling of **19a** with 3-aminobenzenesulfonamide give **2p** under EDC.HCl and TEA coupling condition (Fig. 2B). To synthesize **2n** and **2o**, the acid **19a** had to be converted into an acid chloride with oxalyl chloride before reacting it with the respective amines to form **20n** and **20o**.This was attributed to the conjugative electron-withdrawing effects from the methyl ester on the benzene ring, resulting in a decrease in electron density of the amine which in turn affected its reactivity. As a result, a harsher amidation condition was required. **20n** and **20o** were then hydrolyzed to the free acid **2n** and **2o** in a similar manner (Fig. 2B). **2q** was synthesized by coupling **7a** with **22** followed by hydrogenation and hydrolysis (Fig. 2C).

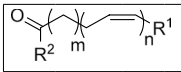								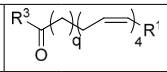						
Cpd	**R^2**	**m**	**n**	**R^1**	**% $cPLA_2$ Activity**	**% Inhibition**	**PSA[a]**	**Cpd**	**R^3**	**q**	**R^1**	**% $cPLA_2$ Activity**	**% Inhibition**	**PSA[a]**
1a	CF_3	2	4	C_5H_{11}	40.0 ± 0.9	60.0	17.1	**2a**	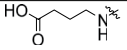	2	C_5H_{11}	39.7 ± 2.6	60.3	66.4
1b	CF_3	2	4	C_3H_7	37.0 ± 3.9	63.0	17.1	**2b**	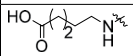	2	C_5H_{11}	26.7 ± 0.1	73.3	66.4
1c	CF_3	2	4	C_8H_{17}	45.0 ± 3.5	55.0	17.1	**2c**	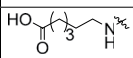	2	C_5H_{11}	40.9 ± 1.1	59.1	66.4
1d	CF_3	2	4	Ph	31.8 ± 2.0	68.2	17.1	**2d**	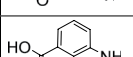	2	C_5H_{11}	13.2 ± 1.2	86.8	66.4
1e	CF_3	1	4	C_6H_{13}	40.5 ± 3.6	59.5	17.1	**2e**	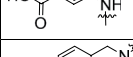	2	C_5H_{11}	25.8 ± 0.1	74.2	66.4
1f	CF_3	2	3	C_5H_{11}	33.8 ± 2.2	66.2	17.1	**2f**	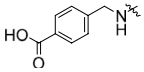	2	C_5H_{11}	35.6 ± 2.1	64.4	66.4
1g	CF_3	2	3	C_3H_7	42.5 ± 0.3	57.5	17.1	**2g**	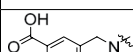	3	C_5H_{11}	15.5 ± 0.3	84.5	66.4
1h	CF_3	2	3	C_8H_{17}	45.6 ± 2.8	54.4	17.1	**2h**	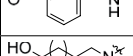	3	C_3H_7	43.6 ± 0.2	56.4	66.4
1i	CF_3	2	2	C_5H_{11}	36.4 ± 3.3	63.6	17.1	**2i**	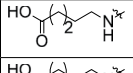	3	C_5H_{11}	11.5 ± 1.0	88.5	66.4
1j	CF_3	2	2	C_7H_{15}	33.9 ± 4.8	66.1	17.1	**2j**	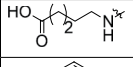	3	C_3H_7	16.5 ± 1.2	83.5	66.4
1k	CF_3	2	2	$C_{11}H_{23}$	54.0 ± 6.9	46.0	17.1	**2k**	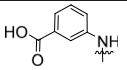	4	C_5H_{11}	37.7 ± 1.5	62.3	66.4
1l	CF_3	2	2	$C_{13}H_{27}$	72.4 ± 12.9	27.6	17.1	**2l**	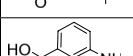	2	C_5H_{11}	67.4 ± 5.7	32.6	72.2
1m	NH_2	2	4	C_5H_{11}	60.7 ± 1.9	39.3	43.1	**2m**	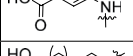	2	C_5H_{11}	57.5 ± 1.4	42.5	72.2
1n	$CClF_2$	2	4	C_5H_{11}	49.2 ± 4.5	50.8	17.1	**2n**	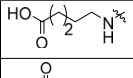	2	C_5H_{11}	33.3 ± 0.9	66.7	66.4
1o	CHF_2	2	4	C_5H_{11}	40.2 ± 0.5	59.8	17.1	**2o**	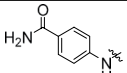	2	C_5H_{11}	65.5 ± 4.0	34.5	66.4
								2p	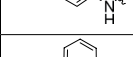	2	C_5H_{11}	53.9 ± 2.7	46.1	89.3
								2q	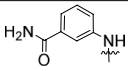	1	C_5H_{11}	56.6 ± 4.9	43.4	66.4
								20c	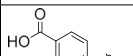	2	C_5H_{11}	84.8 ± 1.0	15.2	55.4

Table 1. Inhibitory activities of **1** and **2** on $cPLA_2$ at 10 μM and their physiochemical properties. [a]Values were obtained from ChemBioDraw Ultra 12.

Testing of inhibitor compounds using $cPLA_2$ assay. Table 1 shows the inhibitory activities of **1** and **2** on $cPLA_2$. The compounds were evaluated with a fluorogenic PLA_2 assay kit (EnzChek® Phospholipase A_2 Assay Kit, Catalog No: E10217) at a standard 10 μM concentration. Potential inhibitors were determined by their ability to lower $cPLA_2$ activity to a greater extent than **1a**.

Modification of the tail length. From Table 1 (Cpd **1a**–**1c** and **1i**–**1l**), varying the tail length did not provide a significant improvement in $cPLA_2$ inhibitory activity as compared to $AACOCF_3$. In fact, increasing the alkyl chain length from C5 (**1i**) to C13 (**1l**) resulted in a significant decrease in $cPLA_2$ inhibition. Replacing the alkyl tail with a phenyl moiety provided **1d** which showed the highest $cPLA_2$ inhibitory activity in the trifluoromethylketone series of compounds. This could be attributed to the additional interactions with $cPLA_2$ (*vide infra*).

Modification of number of double bonds. The skipped alkene functionality in the arachidonyl backbone causes **1a** to be light and oxygen sensitive[36]. We hypothesized that reducing the number of skipped alkenes on the backbone could improve the compound's stability. Hence analogues with a reduced number of double bonds (Table 1 Cpd **1f**–**l**) were synthesized (Fig. 1B,C). However the potencies of these compounds were found to be lower than that of **1a**, indicating that it was more favourable for analogues with the same number of carbons to contain more double bonds (Table 1, Cpd **1a**, **1h** and **1k**). A plausible explanation could be due to the increased rigidity of the compound with more double bonds, making them less rotatable and hence improving their affinity for the enzyme pocket.

Modification of the number of methylene groups between the first double bond and the carbonyl group. Earlier studies have shown that the number of methylene groups between the carbonyl carbon and the first double bond (Fig. 1A) is important for enzyme recognition[37]. To better understand the effects of these methylene groups on the inhibitory properties of the compound, **1e** with two methylene groups was synthesized. Results obtained showed that **1e** had the same $cPLA_2$ inhibitory activity as **1a** (Table 1) suggesting that the position of the double bonds from the carbonyl for enzyme recognition may not be as important as it was previously postulated[37].

Modification of the functionality on the carbonyl group. Earlier studies have shown that the presence of a trifluoromethylketo moiety confers a very high electrophilicity on $AACOCF_3$[38]. This can result in the keto existing largely in the hydrated form, thus reducing the concentration of the active species. To vary the electrophilicity of the carbonyl group, we modulated the number of fluorine atoms or replaced the trifluoro moiety with other functionalities (Table 1, Cpd **1m**–**1o**). However, reducing the electrophilicity of the carbonyl group by reducing the number of fluorine atoms on the trifluoromethyl moiety did not result in a more potent $cPLA_2$ inhibitor (Table 1, Cpd **1n**–**1o**). Similarly a decrease in $cPLA_2$ inhibitory activity was observed in **1m** when the carbonyl was converted into a primary amide. However all the compounds in Table 1 have the same polar surface area (17.1 $Å^2$) except **1m** (43.1 $Å^2$). Since the polar surface area measures the compound's ability to permeate cells, we decided to explore other analogues of **1m** by functionalizing the amide moiety[39–41].

Pickard *et al.*[42] have shown that site-directed mutagenesis of Arg200 in $cPLA_2$ severely affected its catalytic property while molecular docking and crystallography studies by other groups have indicated that Arg200 plays a stabilizing role by interacting with the phosphate group on phosphatidylcholine or the carboxylate groups on $cPLA_2$ inhibitors[43,44]. Through a combination of deuterium exchange mass spectrometry and modeling, Burke and co-workers have also reported the interaction of Arg200 with $cPLA_2$ inhibitors containing carboxyl groups[45]. We thus postulated that functionalizing the amide moiety of **1m** with a negatively charged moiety that interacts with Arg200 could improve the compound's $cPLA_2$ inhibitory activity. Hence various analogues containing an alkyl extension ending with either a carboxylic acid, ester, sulfonamide or amide functionality were synthesized (Fig. 2).

We started the investigation by synthesizing **2a**–**2c** which contained different number of methylene groups between the amide and carboxylic acid functionalities. **2b** was found to possess the best $cPLA_2$ inhibitory activity amongst the three compounds (Table 1 Cpd **2a**–**2c**), suggesting that four methylene groups were optimal between the amide and carboxyl groups. To determine if the interaction between the carboxylic acid functionality and Arg200 was responsible for increasing the compound's $cPLA_2$ inhibitory activity, **20c** containing an ester instead of a carboxylic acid was also prepared. A significant decrease in activity was observed in **20c**, thus confirming the importance of the carboxylic acid moiety.

Next, we directed our efforts to determine the effect of the number of methylene groups between the first double bond and the carbonyl group. Although it was observed in our earlier studies of compound **1** that this effect is insignificant, the presence of a carboxyl-containing extension in **2** would result in a longer molecule than **1**, which could alter the interactions between **2** and the putative binding pocket in $cPLA_2$. Comparison of the activities of **2b**, **2g**, **2k** and **2q** (Table 1) showed that $cPLA_2$ inhibition improved when the number of methylene groups was increased, with four methylene groups (**2g**) between the first double bond and the carbonyl group being the optimal number.

We have also explored rigidifying the compound by replacing the alkyl groups between the amide and carboxylic acid with a phenyl moiety. Three analogues containing a meta- (**2d**), para- (**2n**) and ortho- (**2o**) carboxylic acid were synthesized. **2d** exhibited the best $cPLA_2$ inhibition, providing a 2.5-fold increase in activity. When the carboxylic acid moiety was replaced with an amide or sulfonamide (Table 1), lower $cPLA_2$ inhibitory activities were observed.

Varying the alkyl tail of **2d** provided **2i** and **2j**. **2i** exhibited 88.5% $cPLA_2$ inhibition and is the most potent compound found in this study. Hence from our structure-activity studies, three compounds, **2d**, **2g** and **2i** which significantly decreased the $cPLA_2$ activity were identified. Since **2d** and **2i** are structurally analogous, only the stronger inhibitor **2i** was selected for further studies. The IC_{50} values of **2g** and **2i** were determined to be 5.3 ± 0.3 and $2.9 \pm 0.2\,\mu M$ respectively, indicating that these compounds display 3-fold and 5.5-fold stronger $cPLA_2$ inhibition than **1a** ($IC_{50} = 16.5 \pm 3.0\,\mu M$).

Cell survival test. To explore whether the inhibitors are cytotoxic, MTS assay were conducted on BV-2 cells, a murine microglial cell line derived from post-natal mouse cerebella, and HEK293T cells that are derived from human embryonic kidney. Both cell types were treated with $10\,\mu M$ of **1a**, **2g** and **2i** for 48 h and 72 h (Fig. 3A,B). Dimethyl sulfoxide (DMSO) vehicle control was also included as the compounds were dissolved in DMSO. The amount of DMSO used in the assay was limited to 1% of the total volume to ensure that it does not result in cytotoxicity of cells. Both **2g** and **2i** showed no significant toxic effects on BV-2 and HEK293T cells as compared to vehicle control.

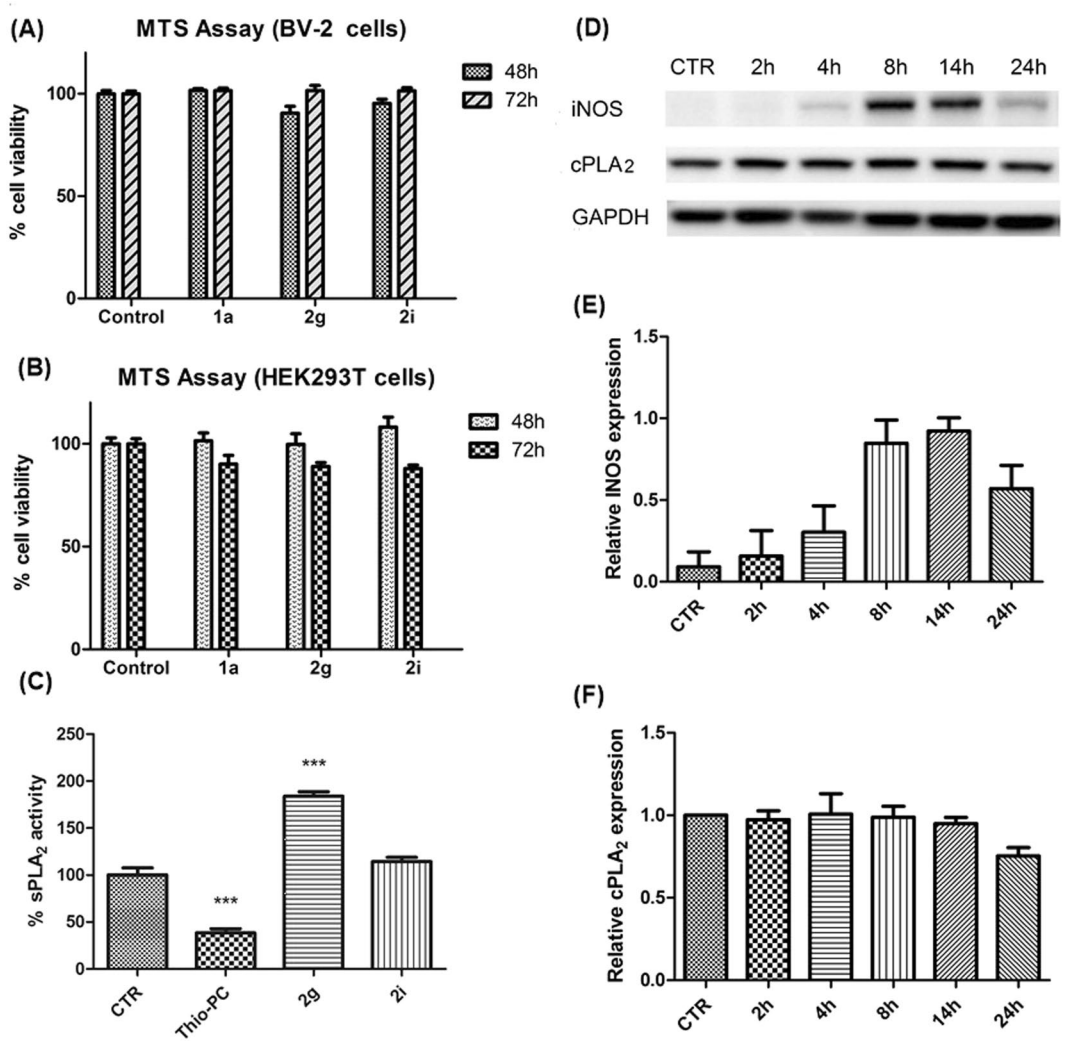

Figure 3. (**A**,**B**) MTS assay conducted on **1a**, **2g** and **2i** on BV-2 and HEK293T cells at different time points. Three independent biological repeat of cells were treated with 10 μM of the compound (final concentration). Data analysed by one-way ANOVA with Bonferroni's Multiple Comparison Test against the Control set indicates no statistical differences in cell survival between the treated and control samples. (**C**) $sPLA_2$ activity of the respective compounds at 10 μM. CTR refers to the DMSO control. Thio-PC refers to the set when $sPLA_2$ selective inhibitor thioetheramide-PC is present. Data analysed by one-way ANOVA with Bonferroni's Multiple Comparison Test against the CTR set indicates significant differences between DMSO control versus Thio-PC and **2g** (***$P < 0.01$). There is no significant difference between DMSO and **2i** indicating **2i** has no $sPLA_2$ inhibitory activity. (**D–F**) Induction of iNOS expression in BV-2 cells after 2 μg/mL of LPS stimulation at different time points. BV-2 cells were collected and lysed at the respective time points and western blot was performed. (**D**) Representative western blot out of 3 independent experiments showing protein expression of iNOS, $cPLA_2$ and GAPDH. Densitometry analysis of (**E**) iNOS and (**F**) $cPLA_2$ after normalization with GAPDH. Uncropped images of blots can be found in Supplementary information Fig. S2.

$sPLA_2$ assay. To further explore their selectivity towards $cPLA_2$, 10 μM of **2g** and **2i** were evaluated for their inhibition against recombinant $sPLA_2$ using the fluorogenic PLA_2 assay (Fig. 3C). Thioetheramide-PC, a specific inhibitor of $sPLA_2$ ($IC_{50} = 2\,\mu M$)[46] was used as a reference and produced a 62% reduction of $sPLA_2$ activity. **2i** did not provide a significant change in $sPLA_2$ activity, indicating that it could not inhibit $sPLA_2$. However, **2g** showed a significant increase of $sPLA_2$ activity to 184%, suggesting that it could possibly be a $sPLA_2$ activator, thereby disqualifying it as a selective $cPLA_2$ inhibitor. With the elimination of **2g**, only **2i** was assessed for its ability to oppose microglia activation via $cPLA_2$ inhibition (there is a possibility of **2i** inhibiting $iPLA_2$. However the purified enzymatically active form of $iPLA_2$ is not commercially available. Hence in this study, we did not evaluate **2i** for its inhibitory activity against $iPLA_2$. Such testing would be important in the future e.g. through the purification of $iPLA_2$ from rat brain lysates to obtain active $iPLA_2$[47]).

LPS stimulation of BV-2 cells triggers iNOS production. It is well-established that reactive oxygen species (ROS) and nitric oxide (NO), produced during microglia activation, contribute to inflammatory response

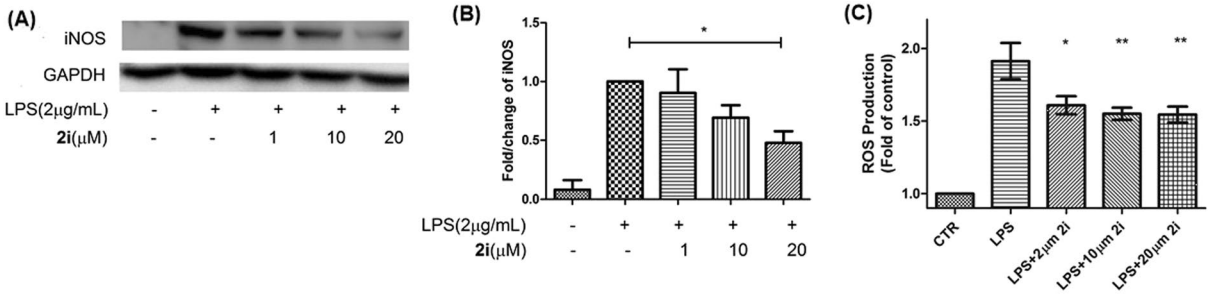

Figure 4. (**A**,**B**) Changes in iNOS protein expression in BV-2 cells after 14 h treatment with 2 μg/mL of LPS and different concentrations of **2i**. BV-2 cells were collected, lysed and western blot was performed. (**A**) Representative western blot out of 3 independent experiments showing protein bands of iNOS and GAPDH. (**B**) Densitometry analysis of iNOS after normalization with GAPDH. Data analysed by one-way ANOVA with Dunnett's Multiple Comparison Test indicates significant difference between LPS treated versus LPS treated with 20 μM of **2i** (*$P < 0.05$). (**C**) **2i** reduces ROS production in BV-2 cells after a 14 h 2 μg/mL LPS insult. Different concentrations of **2i** were dissolved with LPS in culture medium and treated to the cells for 14 h. Five independent biological repeat of cells were conducted. Data analysed by one-way ANOVA with Bonferroni's Multiple Comparison Test indicates significant difference when comparing between LPS-treated versus LPS-treated with different concentrations of **2i** (**$P < 0.01$, *$P < 0.05$). Uncropped images of blots can be found in Supplementary information Fig. S3.

and cytotoxic damage to the surrounding neurons and neighbouring cells[48]. Recent studies have shown that BV-2 microglial cell could serve as an *in vitro* model to mimic such neuroinflammatory states when stimulated with lipopolysaccharide (LPS)[49]. LPS activates BV-2 cells by triggering a cascade of inflammatory events which includes the production of NO. This event is characterized by the generation of the biomarker, inducible nitric oxide synthase (iNOS), as well as ROS. Chuang *et al.*[50] have also shown that $cPLA_2$ is a major contributor in this pathway and inhibiting this enzyme reduces the production of the neurotoxic mediators and provide neuroprotective effects. Therefore to investigate the ability of **2i** in inhibiting $cPLA_2$ in a neuroinflammatory model, BV-2 cells were treated with LPS (2 μg/mL), incubated for different time points, collected and lysed for protein extraction. Western blots conducted showed that iNOS level was highest between 8–14 h (Fig. 3D). Densitometry analyses showed that there were no statistical differences in the iNOS levels between the 8 and 14 h time points (Fig. 3E). The $cPLA_2$ level was also determined and found to be largely constant throughout the entire activation process with a slight drop at the 24 h timepoint (Fig. 3F). Next, **2i** (1, 10 and 20 μM) were incubated together with LPS in the BV-2 cells for 14 h (Fig. 4A,B). The LPS-induced iNOS expression was significantly reduced by 50% when treated with 20 μM of compound **2i**. Varying the concentration of **2i** from 1–20 μM showed a dose-dependent decrease in the iNOS level, indicating that **2i** was capable of reducing iNOS production.

ROS production. CM-H2DCFDA was used as the main detection reagent for ROS for this study. Being a chloromethyl derivative of the conventional H2DCFDA, it is better retained in the cells due to the reaction of its chloromethyl group with intracellular thiol species. In addition, esterase present in the cells would convert the acetate group found in CM-H2DCFDA into carboxylic acid, further retaining it in the cell. To investigate the ROS production by BV-2 cell stimulated with LPS, intracellular ROS was measured 14 h post-stimulation with CM-H2DCFDA fluorescence. A 2-fold increase in ROS was detected as compared to the control. When **2i** (2, 10 and 20 μM) were incubated with the BV-2 cells in the presence of 2 μg/mL LPS for 14 h, a dose-dependent decrease in ROS was observed (Fig. 4C), indicating **2i** could reduce ROS production under neurotoxic conditions. However, residual ROS were observed for samples treated with **2i**. This could be because the activation of ROS production might not be solely due to the inflammatory pathway mechanism involving $cPLA_2$. It was reported in previous studies that a multitude of several other processes producing ROS may be at work[51,52].

***In vitro* evaluation of the blood-brain-barrier (BBB) permeation.** A major requirement for the development of a successful drug for the treatment of central nervous system (CNS) disorder is its ability to pass through the BBB to reach the therapeutic target. Hence screening for its ability to penetrate the BBB is of great importance.

Earlier studies[53] have demonstrated that the parallel artificial membrane permeation assay (PAMPA)[53] assay provides good prediction of *in vivo* BBB permeability and is a useful tool to screen compounds for brain penetration. Thus to explore whether **2i** is able to penetrate into the brain, we used PAMPA with porcine brain lipids as the lipid barrier. Commercially available and highly potent $cPLA_2$ inhibitors, CDIBA (an analogue of efipladib)[12] and pyrrophenone, were also evaluated for their ability to penetrate the BBB. The effective permeability (P_e) of **2i**, CDIBA and pyrrophenone were found to be $12.34 \pm 1.46 \times 10^{-6}$, $3.98 \pm 0.24 \times 10^{-6}$ and $2.00 \pm 0.05 \times 10^{-6}$ cm/s (16 h, 25 °C). P_e values of reference compounds determined under similar conditions were of the order propranolol > carbamazepine > quinidine > caffeine > dopamine, which agreed with reported literature[54,55]. A minimum P_e of 7×10^{-6} cm/s has been cited as the threshold for permeability across the blood brain barrier[56]. As the P_e of **2i** exceeded this value, we are optimistic that **2i** has the potential to transverse the BBB. We also found good aqueous

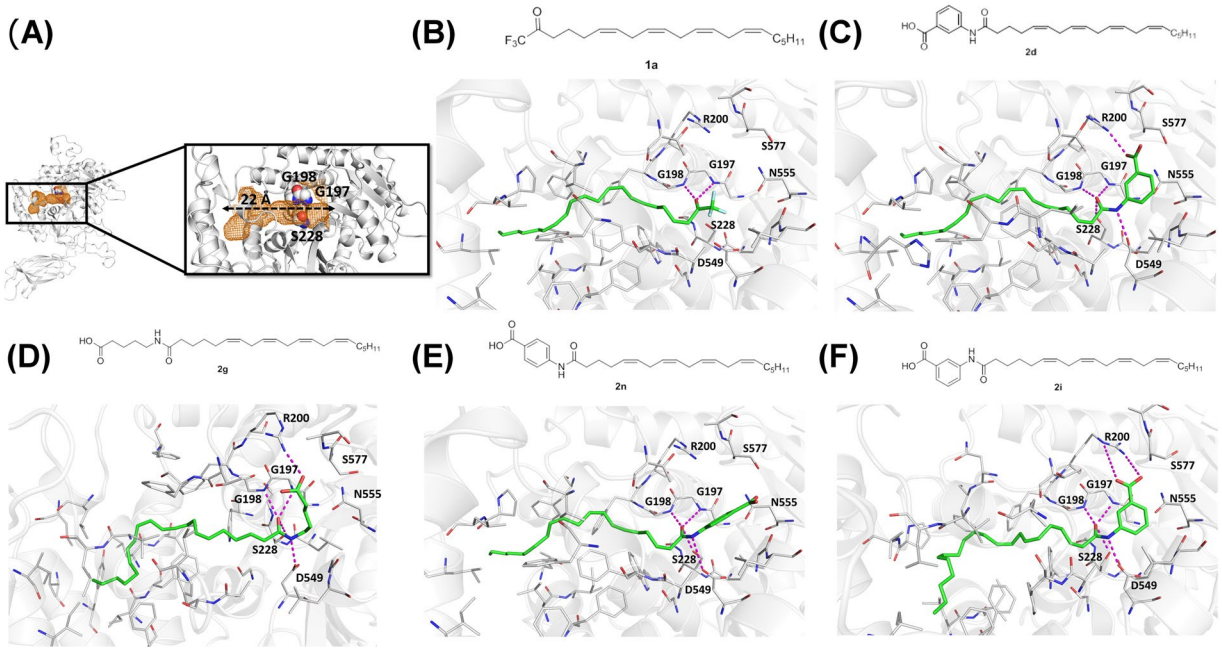

Figure 5. (**A**) Crystal structures of $cPLA_2$ derived from 1CJY. Cartoon representations of the overall structure of the $cPLA_2$ (left). Inhibitor binding site on the $cPLA_2$ (right). Residues Ser228 (S228), Gly197 (G197), Gly198 (G198) are highlighted. Binding site is shown as mesh (orange). Predicted binding mode of **1a** (**B**), **2d** (**C**), **2g** (**D**), **2n** (**E**), **2i** (**F**) docked into $cPLA_2$ with key interacting residues highlighted. Residues in the active sites are shown as lines; hydrogen bonds are indicated by dashed lines (magenta); protein residues involved in hydrogen bond interactions are labelled accordingly.

solubility (>100 μM, 24 h, 25 °C) for **2i** at pH 7.4. Taken together, the promising physicochemical profile of **2i** warrants continued attention on this compound as an inhibitor of $cPLA_2$.

***In-silico* docking analysis.** A docking study was performed to rationalize the inhibitory activities and to identify the possible binding sites of **2g** and **2i** on the $cPLA_2$ enzyme. The crystal structure of $cPLA_2$ in its apo form (PDB ID 1CJY, resolution 2.5 Å) and with a few missing regions was obtained from the protein data bank[57]. The missing regions were modelled and the complete structure was subjected to molecular dynamics (MD) simulations (as outlined in Methods). The complete model of $cPLA_2$ remained stable during the simulation. The conformations sampled during the last 50 ns of the MD simulations were clustered into conformational sub-states using the Kclust program from the MMTSB tool set, with an rmsd of 2 Å set as cutoff. The cluster centroids of the top 5 most populated clusters were used for docking calculations.

Docking calculations identified a $cPLA_2$ binding site around the catalytically important residue Ser228[43,44]. This binding site was shown to be highly negatively charged on one end and slightly positively charged on the other end. Both these charged ends are connected by a 22 Å long, narrow tunnel that is made up of hydrophobic amino acids (Fig. 5A). The $cPLA_2$ binding site was calculated to have a total volume of ~205 $Å^3$. Since there are no co-crystal structures of $cPLA_2$-inhibitor available, various analogues of **1** and **2** were docked and the results obtained were compared to the experimental data to understand the binding of the compounds.

Docking calculations with **1a** showed the compound penetrating into the deep hydrophobic pocket of $cPLA_2$ and the carbonyl group interacting with Ser228 via hydrogen bonds and van der Waals contacts (Fig. 5B). Using this docking protocol, analogues of **1** and **2** were docked around this region with different conformations of $cPLA_2$ identified through clustering the MD simulation trajectories. Ten poses for each compound were computed and the best docking pose for each compound was chosen by ranking the computed binding energy (docking score). Analysis of the top scored solutions (lowest energy solutions) showed that all the compounds bind similarly in the active sites of $cPLA_2$ with (i) the electrophilic carbon of the substituted ketone in **1** or amide in **2** being in close proximity to Ser228, and (ii) Gly197/Gly198 interacting with the carbonyl oxygen of **1** or the amide oxygen of **2**. In addition, docking analysis of **2** shows the carboxylic acid moiety interacting with the side chains of Arg200. For the aminobenzoic acid analogues **2d** and **2n**, the carboxylic acid functionality is in closer proximity to Arg200 when it is in the meta position than the para position (Fig. 5C,E). This indicates a stronger attractive interaction which could contribute to the stronger inhibitory property of **2d**. Furthermore, the interactions between the carboxylic acid moiety and Arg200 provide a tighter binding for **2g** and **2i** than **1a** (Fig. 5D,F). **2i** which has its carboxylic acid moiety closest to Arg200, has the most favorable interaction with $cPLA_2$. These results corroborated with our experimental $cPLA_2$ inhibition assay data which show **2i** as the strongest $cPLA_2$ inhibitor.

Conclusion

$cPLA_2$ activation has been shown to be critically important in the regulation of homeostatic processes and disease pathogenesis. Therefore, $cPLA_2$ represents a potential novel therapeutic target to treat a wide range of diseases from cancer to neurodegenerative diseases such as Alzheimer's disease and multiple sclerosis[8,58]. In our efforts to develop potential drug candidates to treat neurological disorders, we have synthesized a new class of AA analogues and identified one compound, **2i** that is a non-cytotoxic, $cPLA_2$-selective inhibitor which inhibits the enzyme more potently than $AACOCF_3$. Computational modelling and extensive simulations support the ability of **2i** to dock into the active site of $cPLA_2$. **2i** is predicted to be brain penetrant through our PAMPA assay and is able to reduce ROS and NO production in LPS-stimulated BV-2 microglial cells. Further studies are presently ongoing to develop the compound as a lead compound. Understanding its *in vivo* effect will be crucial in evaluating its clinical potential.

Methods

Synthesis of 1 and 2. Detailed experimental procedures and compound characterization data can be found in the supplementary information, available in the online version of the paper.

Enzchek phospholipase A_2 fluorogenic assay (% activity). The assay was conducted according to the manufacturer's instruction (E10217, Molecular Probes) with slight modification. Briefly, substrate solution was separately prepared by mixing 5 μL of DOPG, 5 μL of DOPC and 5 μL of substrate respectively in 1.5 mL of 1X phospholipase A_2 reaction buffer. The mixture was vortexed vigorously for 3 min before allowing to stand at room temperature for 1 h. 48 μL of 1X phospholipase A_2 reaction buffer were added into each well of a 96-wells plate. This was followed by addition of 1 μL of recombinant $cPLA_2$ (P4074-03R, US Biological) and 1 μL of 1 mM of the respective compound dissolved in DMSO. The final concentration of the test compound achieved is 10 μM. The reaction was initiated by adding 50 μL of the substrate solution and incubating at room temperature for 1 h. Fluorescence was measured using a Varioskan plate reader (Thermo Scientific, MA, USA) by exciting at 485 nm, while fluorescence emission was detected at 515 nm. Positive control was performed when 1 μL of test compound was replaced by vehicle DMSO. % activity was expressed as the mean value of duplicate wells from three experiments. % activity was calculated by the following formula

$$\%activity = \frac{fluorescence\ of\ tested\ well - background}{fluorescence\ of\ postive\ control - background} \quad (1)$$

Enzchek phospholipase A_2 fluorogenic assay (IC_{50}). The assay was conducted as described above. Instead of adding a fixed concentration of the test compound, various concentrations of compound were reconstituted in DMSO. 48 μL of 1X phospholipase A_2 reaction buffer were added into each well of a 96-wells plate. This was followed by addition of 1 μL of recombinant $cPLA_2$ (P4074-03R, US Biological) and 1 μL of the respective concentration of the test compound dissolved in DMSO. The reaction was initiated by adding 50 μL of the substrate solution and incubating at room temperature for 1 h. Fluorescence was measured using a Varioskan plate reader by exciting at 485 nm, while fluorescence emission was detected at 515 nm. Positive control was performed when 1 μL of test compound was replaced by vehicle DMSO. IC_{50} was expressed as the mean value of duplicate wells from three experiments.

Enzchek phospholipase A_2 fluorogenic assay (selectivity). The assay was conducted as described above. Instead of adding $cPLA_2$, it was replaced by $sPLA_2$. 48 μL of 1X phospholipase A_2 reaction buffer was added into each well of a 96-wells plate. This was followed by addition of 1 μL of $sPLA_2$, human recombinant type V (10009563, Cayman Chemical) and 1 μL of 1 mM of the respective compound or thioetheramide-PC (62750, Cayman Chemical) dissolved in DMSO. The final concentration of the test compound achieved is 10 μM. The reaction was initiated by adding 50 μL of the substrate solution and incubating at room temperature for 1 h. Fluorescence was measured using a Varioskan plate reader by exciting at 485 nm, while fluorescence emission was detected at 515 nm. Positive control was performed when 1 μL of test compound was replaced by vehicle DMSO. % activity was expressed as the mean value of duplicate wells from four experiments. % activity was calculated by the following formula:

$$\%activity = \frac{fluorescence\ of\ tested\ well - background}{fluorescence\ of\ postive\ control - background} \quad (2)$$

Cell-culture and LPS treatment. Murine BV-2 cells were cultured in DMEM (11965092, ThermoFisher Scientific) supplemented with 10% fetal bovine serum, 100 μg/mL streptomycin and 100 units/mL penicillin. Cells were maintained in an incubator at 37 °C, under a 5% CO_2 and in a water saturated environment. When performing LPS treatment, BV-2 cells were plated on a 10 cm dish in 10 mL culture medium at a density of 1×10^6 cells per dish one day prior to the experiment. After observing that cells were at 90% confluency, lipopolysaccharide (L6529, Sigma) pre-dissolved in culture medium to achieve a concentration of 2 μg/mL was added to the dish. Different concentrations of test compounds in DMSO were added to the LPS containing medium which was then transferred to the 10 cm dish. DMSO was used as a vehicle control and added to the non-LPS treated control. The cells were incubated at 37 °C, under a 5% CO_2 environment. After the respective timepoints, cells were washed once with 1xPBS (10 mL) and scrapped on ice with 8 mL 1xPBS. Collected cells were centrifuged at 800 rpm for 3 min at 4 °C, before discarding the supernatant. Cells were lysed by RIPA buffer supplemented with 1× protease inhibitor (Roche) and 1 mM PMSF and incubated under ice for 30 min. This was followed by pelleting the cell

debris at 4 °C for 30 min at 13200 rpm before transferring the supernatant to a clean tube and storing the sample at −20 °C. Three independent biological repeats were performed.

MTS cell proliferation assay. Cells were plated on a 96-wells plate and grown for 24 h to a density of 8000 cells per well for both HEK293T and BV-2 cells. Cells were cultured at 37 °C under a 5% CO_2 environment in 100 μL of culture medium. Thereafter, the compound of interest dissolved in culture medium at a concentration of 10 μM was replaced into each well. DMSO was added as vehicle in the control group. 3 biological replicates were performed. The plates were then incubated at 37 °C with 5% CO_2 for 48 h and 72 h. At each individual time point, 20 μL of CellTiter 96® AQueous One Solution (MTS reagent) was added into each well and re-incubated at 37 °C with 5% CO_2 without light for 3 h. Colorimetric readings were taken using a Varioskan plate reader at 490 nm and analyzed. Three independent biological repeats with four technical replicates were performed.

BCA Assay. BCA assay (23225, Pierce BCA Protein Assay Kit) was performed to quantify the concentration of proteins in the cell lysate. 10 μL of test samples (1 μL with 9 μL of lysis buffer) and BSA standards (range from 1.25 to 50 μg/ml) were mixed in a 96 well-plate and incubated with 190 μL of working reagent mixture (Ratio of Reagent A:B used was 50:1) at 37 °C for 20 min. The colour intensity that was developed was read at 562 nm using a spectrophotometer. A standard curve of different concentrations of BSA was plotted using the average blank-corrected readings for each standard *vs*. its respective concentration (μg/ml). This was then used to determine the protein concentration for unknown samples.

Western Blot. 25 μg of individual protein samples were mixed with an equal volume of 2x Laemmli buffer containing DTT and denatured at 90 °C for 10 min. The lysates were ran in a 10% tris-glycine SDS-PAGE gel at 100 V for 1.5 h in 1x tris-glycine running buffer. The protein samples on the gel were then transferred onto a PVDF membrane. The membranes were then blocked for 1 h at room temperature in 5% skim milk in 1x TBS-0.1% Tween 20 (TBST), followed by overnight incubation with the respective primary antibody dissolved in 5% milk in TBST at 4 °C. Secondary detection were conducted with a secondary horse-radish peroxidase-conjugated antibody (1:10000) dissolved in 5% skim milk in TBST for 1 h at room temperature. Enhanced chemiluminescence (ECL) detection of protein bands was performed using ECL Plus Western Blotting detecting system (GE Healthcare). Antibodies used in western blot include rabbit polyclonal anti-NOS2 (Santa-Cruz, sc-651, 1:100), mouse monoclonal anti-$cPLA_2$ primary antibody (Santa Cruz, sc-454, 1:200), mouse monoclonal anti-GAPDH (Merck, 1:10000), with secondary horse-radish peroxidase-conjugated antibodies (Santa Cruz, 1:10000).

ROS assay. 20,000 BV-2 cells were seeded into a 96-well plate in 100 uL of culture medium and allowed to grow overnight. When a 90% cell confluency was observed, lipopolysaccharide pre-dissolved in culture medium to achieve a concentration of 2 μg/mL was added to each well of the 96 well. Different concentrations of test compounds in DMSO were added to the LPS containing medium and was then transferred to the cells. DMSO was used as vehicle control and added to the non-LPS treated control. The cells were incubated for 14 h at 37 °C, under a 5% CO_2 environment. Medium were removed and washed once with 1x HBSS. 100 μL of 10 μM CM-H2DCFDA (C6827, Molecular Probes) in 1x HBSS solution was added into each well and incubated at 37 °C for 1 h. Fluorescence detection was done by exciting the dye at 485 nm and detection of emission at 525 nm. Five independent biological repeats with six technical replicates were conducted.

Solubility determinations. Solubility determinations were carried out on Multiscreen® Solubility filter plates (Millipore-MSSLBPC10) from Millipore Corporation (MA, USA) following the protocol (PC2445EN00) from the manufacturer.

Determination of permeability. The Parallel Artificial Membrane Permeability Assay (PAMPA) was used to determine the effective permeability (P_e) of **2i**. The method reported by Di *et al.*[53] was followed with modifications. Determinations were carried out on MultiScreen-IP PAMPA assay (donor) plates (MAIPNTR10) and MultiScreen Receiver Plates (MATRNPS50) from Millipore Corporation (USA) with porcine polar brain lipids (Avanti Polar Lipids Inc, Alabaster, AL) as the lipid barrier.

An aliquot (5 μL) of 2% porcine brain lipids in dodecane (ReagentPlus®, Sigma Aldrich, USA) was dispensed into the donor well. A stock solution (5 mM) of **2i** prepared in DMSO was diluted with 1x phosphate buffer (PBS, pH 7.4) to give a 50 μM solution. An aliquot (300 μL) of the solution was dispensed into the donor well and an equal volume of buffer (1xPBS with 1% DMSO) was added to the corresponding acceptor well. The donor and acceptor plates were assembled, the unit was placed in a humidified box and gently agitated on a mini shaker at room temperature (25 °C) for 16 h. After this time, aliquots (200 μL) were withdrawn from the donor and acceptor wells, diluted separately to 1 mL with PBS, and quantified at λmax of 290 nm on a Shimadzu UV-1800 Spectrophotometer.

The PAMPA permeabilities of standards (caffeine, quinidine, carbamazepine, dopamine and propanolol) were determined under similar conditions. 300 μL aliquots of stock solutions (500 μM, 1xPBS, 0.1% DMSO) were dispensed to donor wells as described earlier. Quantification was by UV at λmax of 272 nm (caffeine), 284 nm (carbamazepine), 330 nm (quinidine), 280 nm (dopamine) and 288 nm (propanolol). Calibration plots of standards were determined under similar analytical conditions. The effective permeability (Pe) of these compounds have been reported to vary in the sequence propranolol (most permeable) > carbamazepine > quinidine > caffeine > dopamine (least permeable)[54,55] and was verified experimentally in our hand. P_e was obtained from (3):

$$Pe = -2.303 \times \{V_A V_D/[(V_A + V_D) \times A \times t]\} \times \log\{1 - [(V_A + V_D)/(V_D \cdot S)] \times C_{A(t)}/C_{D(0)}\} \quad (3)$$

where V_A and V_D are the volumes of acceptor (cm^3) and donor (cm^3) wells respectively, A is the area of the surface area of the membrane (0.24 cm^2), t is the permeation time (s). The P_e of each compound was obtained from at least 3 separate experiments using 2 different stock solutions. For each independent determination, triplicates (3 wells) were run for each compound.

***In silico* docking analysis.** Details on protein modeling, ligand preparation and ligand docking can be found in the supplementary information, available in the online version of the paper.

Data Availability. All data generated or analysed during this study are included in this published article (and its Supplementary Information files).

References

1. Burke, J. E. & Dennis, E. A. Phospholipase A_2 biochemistry. *Cardiovasc. Drugs Ther.* **23**, 49–59 (2009).
2. Calder, P. C. The relationship between the fatty acid composition of immune cells and their function. *Prostaglandins Leukot. Essent. Fat. Acids* **79**, 101–108 (2008).
3. Gentile, M. T. *et al*. Role of cytosolic calcium-dependent phospholipase A_2 in Alzheimer's disease pathogenesis. *Mol. Neurobiol.* **45**, 596–604 (2012).
4. Last, V., Williams, A. & Werling, D. Inhibition of cytosolic phospholipase A_2 prevents prion peptide-induced neuronal damage and co-localisation with beta iii tubulin. *BMC Neuroscience* **13**, 106 (2012).
5. Stephenson, D. *et al*. Cytosolic phospholipase A_2 is induced in reactive glia following different forms of neurodegeneration. *Glia* **27**, 110–128 (1999).
6. Rao, J. S., Kellom, M., Reese, E. A., Rapoport, S. I. & Kim, H.-W. Dysregulated glutamate and dopamine transporters in postmortem frontal cortex from bipolar and schizophrenic patients. *J. Affect. Disord.* **136**, 63–71 (2012).
7. Chalimoniuk, M. *et al*. Involvement of multiple protein kinases in $cPLA_2$ phosphorylation, arachidonic acid release, and cell death in *in vivo* and *in vitro* models of 1-methyl-4-phenylpyridinium-induced parkinsonism – the possible key role of PKG. *J. Neurochem.* **110**, 307–317 (2009).
8. Sun, G. Y. *et al*. Integrating cytosolic phospholipase A_2 with oxidative/nitrosative signaling pathways in neurons: A novel therapeutic strategy for AD. *Mol. Neurobiol.* **46**, 85–95 (2012).
9. Sanchez-Mejia, R. O. *et al*. Phospholipase A_2 reduction ameliorates cognitive deficits in a mouse model of Alzheimer's disease. *Nature Neurosci.* **11**, 1311–1318 (2008).
10. McKew, J. C. *et al*. Indole cytosolic phospholipase $A_2\alpha$ inhibitors: discovery and *in vitro* and *in vivo* characterization of 4-{3-[5-chloro-2-(2-{[(3,4-dichlorobenzyl)sulfonyl]amino}ethyl)-1-(diphenylmethyl)-1H-indol-3-yl]propyl}benzoic acid, Efipladib. *J. Med. Chem.* **51**, 3388–3413 (2008).
11. Seno, K. *et al*. Pyrrolidine inhibitors of human cytosolic phospholipase A(2). *J. Med. Chem.* **43**, 1041–1044 (2000).
12. Ono, T. *et al*. Characterization of a novel inhibitor of cytosolic phospholipase A2α, pyrrophenone. *Biochem. J.* **363**, 727–735 (2002).
13. Ludwig, J., Bovens, S., Brauch, C., Elfringhoff, A. S. & Lehr, M. Design and synthesis of 1-indol-1-yl-propan-2-ones as inhibitors of human cytosolic phospholipase A2α. *J. Med. Chem.* **49**, 2611–2620 (2006).
14. Drews, A. *et al*. 1-(5-Carboxyindol-1-yl)propan-2-one inhibitors of human cytosolic phospholipase A2α with reduced lipophilicity: synthesis, biological activity, metabolic stability, solubility, bioavailability, and topical *in vivo* activity. *J. Med. Chem.* **53**, 5165–5178 (2010).
15. Kokotou, M. G. *et al*. Inhibitors of phospholipase A2 and their therapeutic potential: an update on patents (2012–2016). *Expert Opin. Ther. Pat.* **27**, 217–225 (2017).
16. Kokotou, M. G. *et al*. 2-Oxoesters: a novel class of potent and selective inhibitors of cytosolic group IVA phospholipase A_2. *Sci. Rep.* **7**, 7025 (2017).
17. Nickerson-Nutter, C. L. *et al*. The $cPLA_2\alpha$ inhibitor efipladib decreases nociceptive responses without affecting PGE_2 levels in the cerebral spinal fluid. *Neuropharmacol.* **60**, 633–641 (2011).
18. Ong, W. Y., Farooqui, T., Kokotos, G. & Farooqui, A. A. Synthetic and natural inhibitors of phospholipase A_2: their importance for understanding and treatment of neurological disorders. *ACS Chem. Neurosci.* **6**, 814–831 (2015).
19. Gijón, M. A. & Leslie, C. C. Regulation of arachidonic acid release and cytosolic phospholipase A2 activation. *J. Leukoc. Biol.* **65**, 330–336 (1999).
20. Gijón, M. A., Spencer, D. M., Siddiqi, A. R., Bonventre, J. V. & Leslie, C. C. Cytosolic phospholipase A_2 is required for macrophage arachidonic acid release by agonists that do and do not mobilize calcium. *J. Biol. Chem.* **275**, 20146–20156 (2000).
21. Riendeau, D. *et al*. Arachidonyl trifluoromethyl ketone, a potent inhibitor of 85-kDa phospholipase A2, blocks production of arachidonate and 12-hydroxyeicosatetraenoic acid by calcium ionophore-challenged platelets. *J. Biol. Chem.* **269**, 15619–15624 (1994).
22. Fabian, F. & Lehr, M. Normal-phase HPLC and HPLC–MS studies of the metabolism of a cytosolic phospholipase $A2_\alpha$ inhibitor with activated ketone group by rat liver microsomes. *J. Pharm. Biomed. Anal.* **43**, 601–605 (2007).
23. Kim, E. *et al*. Anti-vascular effects of the cytosolic phospholipase A2 inhibitor AVX235 in a patient-derived basal-like breast cancer model. *BMC Cancer* **16**, 191 (2016).
24. Sundaram, J. R. *et al*. Cdk5/p25-induced cytosolic PLA2-mediated lysophosphatidycholine production regulates neuroinflammation and triggers neurodegeneration. *J. Neurosci.* **32**, 1020–1034 (2012).
25. Yeo, J. F., Ong, W. Y., Ling, S. F. & Farooqui, A. A. Intracerebroventricular injection of phospholipases A_2 inhibitors modulates allodynia after facial carrageenan injection in mice. *Pain* **112**, 148–155 (2004).
26. Kalyvas, A. & David, S. Cytosolic phospholipase a_2 plays a key role in the pathogenesis of multiple sclerosis-like disease. Neuron **41**, 323−335 (2004).
27. Lapitskaya, M. A., Vasiljeva, L. L. & Pivnitsky, K. K. A chemoselective synthesis of functionalized 1,4-alkadiynes (skipped diacetylenes). *Synthesis* 65–66 (1993).
28. Durand, S., Parrain, J.-L. & Santelli, M. A large scale and concise synthesis of γ-linolenic acid from 4-chlorobut-2-yn-1-ol. *Synthesis* 1015–1018 (1998).
29. Jeffery, T., Gueugnot, S. & Linstrumelle, G. An efficient route to skipped diynes and triynes, (Z,Z) dienes and (Z,Z,Z) trienes. *Tetrahedron Lett.* **33**, 5757–5760 (1992).
30. Qi, L., Meijler, M. M., Lee, S. H., Sun, C. & Janda, K. D. Solid-phase synthesis of anandamide analogues. *Org. Lett.* **6**, 1673–1675 (2004).
31. Singh, R. P., Cao, G., Kirchmeier, R. L. & Shreeve, J. M. Cesium fluoride catalyzed trifluoromethylation of esters, aldehydes, and ketones with (trifluoromethyl)trimethylsilane. *J. Org. Chem.* **64**, 2873–2876 (1999).
32. Krishnamurti, R., Bellew, D. R. & Prakash, G. K. S. Preparation of trifluoromethyl and other perfluoroalkyl compounds with (perfluoroalkyl)trimethylsilanes. *J. Org. Chem.* **56**, 984–989 (1991).
33. Reeves, J. T. *et al*. Trifluoromethyl ketones from enolizable carboxylic acids via enediolate trifluoroacetylation/decarboxylation. *J. Org. Chem.* **73**, 9476–9478 (2008).

34. Boivin, J., Kaim, L. E. & Zard, S. Z. An expedient access to trifluromethyl ketones from carboxylic acids. *Tetrahedron Lett.* **33**, 1285–1288 (1992).
35. Ackermann, E. J., Conde-Frieboes, K. & Dennis, E. A. Inhibition of macrophage Ca^{2+} -independent phospholipase A2 by bromoenol lactone and trifluoromethyl ketones. *J. Biol. Chem.* **270**, 445–450 (1995).
36. Porter, N. A., Lehman, L. S., Weber, B. A. & Smith, K. Unified mechanism for polyunsaturated fatty acid autoxidation. Competition of peroxy radical hydrogen atom abstraction,.beta. -*scission, and cyclization. J. Am. Chem. Soc.* **103**, 6447–6455 (1981).
37. Connolly, S. *et al*. Design and synthesis of a novel and potent series of inhibitors of cytosolic phospholipase A_2 based on a 1,3-disubstituted propan-2-one skeleton. *J. Med. Chem.* **45**, 1348–1362 (2002).
38. Street, I. P. *et al*. Slow- and tight-binding inhibitors of the 85-kDa human phospholipase A2. *Biochemistry* **32**, 5935–5940 (1993).
39. Palm, K. *et al*. Correlation of drug absorption with molecular surface properties. *J. Pharm. Sci.* **85**, 32–39 (1996).
40. Kelder, J. *et al*. Polar molecular surface as a dominating determinant for oral absorption and brain penetration of drugs. *Pharm. Res.* **16**, 1514–1519 (1999).
41. van der Waterbeemd, H., Camenisch, G., Chretien, J. R. & Raevsky, O. A. Estimation of blood-brain barrier crossing of drugs using molecular size and shape, and H-bonding descriptors. *J. Drug Target* **6**, 151–165 (1998).
42. Pickard, R. T. *et al*. Identification of essential residues for the catalytic function of 85-kDa cytosolic phospholipase A_2. *J. Biol. Chem.* **271**, 19225–19231 (1996).
43. Dessen, A. *et al*. Crystal structure of human cytosolic phospholipase $a_2$reveals a novel topology and catalytic mechanism. *Cell* **97**, 349–360 (1999).
44. Mouchlis, V. D. *et al*. Binding conformation of 2-oxoamide inhibitors to Group IVA cytosolic phospholiase A_2 determined by molecular docking combined with molecular dynamics. *J. Chem. Inf. Model.* **52**, 243–254 (2012).
45. Burke, J. E. *et al*. Location of inhibitors bound to Group IVA phospholipase A_2 determined by molecular dynamics and deuterium exchange mass spectrometry. *J. Am. Chem. Soc.* **131**, 8083–8091 (2009).
46. Yu, L., Deems, R. A., Hajdu, J. & Dennis, E. A. The interaction of phospholipase A_2 with phospholipid analogues and inhibitors. *J. Biol. Chem.* **265**, 2657–2664 (1990).
47. Yang, H.-C. *et al*. Group-specific assays that distinguish between the four major types of mammalian phospholipase A_2. *Anal. Biochem.* **269**, 278–288 (1999).
48. Di Penta, A. *et al*. Oxidative stress and proinflammatory cytokines contribute to demyelination and axonal damage in a cerebellar culture model of neuroinflammation. *PLoS One* **8**, e54722 (2013).
49. Yao, L. *et al*. Toll-like receptor 4 mediates microglial activation and production of inflammatory mediators in neonatal rat brain following hypoxia: role of TLR4 in hypoxic microglia. *J. Neuroinflammation* **10**, 23 (2013).
50. Chuang, D. Y. *et al*. Cytosolic phospholipase A_2 plays a crucial role in ROS/NO signaling during microglial activation through the lipoxygenase pathway. *J. Neuroinflammation* **12**, 199 (2015).
51. Hsu, H.-Y. & Wen, M.-H. Lipopolysaccharide-mediated reactive oxygen species and signal transduction in the regulation of interleukin-1 gene expression. *J. Biol. Chem.* **277**, 22131–22139 (2002).
52. Gao, F., Chen, D., Hu, Q. & Wang, G. Rotenone directly induces BV2 Cell Activation via the p38 MAPK pathway. *PLOS One* **8**, 72046 (2013).
53. Di, L. *et al*. High throughput artificial membrane permeability assay for blood-brain barrier. *Eur. J. Med. Chem.* **38**, 223–232 (2003).
54. Avdeef, A. *et al*. PAMPA – critical factors for better predictions of absorption. *J. Pharm. Sci.* **96**, 2893–2909 (2007).
55. Liu, H. *et al*. *In vitro* permeability of poorly aqueous soluble compounds using different solubilizers in the PAMPA assay with liquid chromatography/mass spectrometry detection. *Pharm. Res.* **20**, 1820–1826 (2003).
56. Bicker, J. *et al*. A new PAMPA model using an in-house brain lipid extract for screening the blood-brain barrier permeability of drug candidates. *Int. J. Pharm.* **501**, 102–111 (2016).
57. PDB ID: 1CJY, http://dx.doi.org/10.2210/pdb1cjy/pdb.
58. Love, R. $cPLA_2$: common link in the pathogenesis of multiple sclerosis. *Lancet Neurol.* **3**, 199 (2004).

Acknowledgements

The authors thank the Ministry of Education (Singapore) (MoE Tier 2: R-143-000-589-112, MoE Tier 1: R-184-000-272-114) and NMRC (NMRC-1222-2009) for the financial support and the National University of Singapore for a Ph.D scholarship to C.Y.N. The authors also thank the Drug Development Unit (DDU), NUS for their contributions in this project.

Author Contributions

C.Y.N. synthesized and characterized all the compounds with the assistance of W.Y.O. C.Y.N. evaluated the compounds using $cPLA_2$ and $sPLA_2$ assays and conducted the cell survival test and iNOS and ROS production analyses with the assistance of F.C.K.T. S.K. performed the *in-silico* docking analysis. Y.J.C. and M.L.G. performed the BBB permeation analysis. C.Y.N., S. K., F.C.K.T., M.L.G., C.S.V., C.-M.L. and Y.L. analyzed the results and wrote the manuscript.

Additional Information

Supplementary information accompanies this paper at https://doi.org/10.1038/s41598-017-13996-8.

Competing Interests: The authors declare that they have no competing interests.

Publisher's note: Springer Nature remains neutral with regard to jurisdictional claims in published maps and institutional affiliations.